### Title

Probing the Hydrogen Bonding of the Ferrous-NO Heme Center of nNOS by Pulsed Electron Paramagnetic Resonance.




### Journal

Journal of Physical Chemistry A, 119(25)



### Authors

Astashkin, Andrei
Chen, Li
Elmore, Bradley
et al.



### Publication Date

2015-06-25

### DOI

10.1021/acs.jpca.5b01804

Peer reviewed

HHS Public Access

Author manuscript

*J Phys Chem A*. Author manuscript; available in PMC 2015 August 12.

Published in final edited form as:

*J Phys Chem A*. 2015 June 25; 119(25): 6641–6649. doi:10.1021/acs.jpca.5b01804.

# Probing the Hydrogen Bonding of the Ferrous–NO Heme Center of nNOS by Pulsed Electron Paramagnetic Resonance

**Andrei V. Astashkin**[†], **Li Chen**[‡], **Bradley O. Elmore**[‡], **Deepak Kunwar**[‡], **Yubin Miao**[‡], **Huiying Li**[§], **Thomas L. Poulos**[§], **Linda J. Roman**[‖], and **Changjian Feng**[*,‡]

[†]Department of Chemistry and Biochemistry, University of Arizona, Tucson, Arizona 85721, United States

[‡]College of Pharmacy, University of New Mexico, Albuquerque, New Mexico 87131, United States

[§]Departments of Molecular Biology and Biochemistry, Chemistry, and Pharmaceutical Sciences, University of California, Irvine, Irvine, California 92697-3900, United States

[‖]Department of Biochemistry, University of Texas Health Science Center in San Antonio, San Antonio, Texas 78229, United States

## Abstract

Oxidation of L-arginine (L-Arg) to nitric oxide (NO) by NO synthase (NOS) takes place at the heme active site. It is of current interest to study structures of the heme species that activates $O_2$ and transforms the substrate. The NOS ferrous–NO complex is a close mimic of the obligatory ferric (hydro)peroxo intermediate in NOS catalysis. In this work, pulsed electron–nuclear double resonance (ENDOR) spectroscopy was used to probe the hydrogen bonding of the NO ligand in the ferrous–NO heme center of neuronal NOS (nNOS) without a substrate and with L-Arg or *N*-hydroxy-L-arginine (NOHA) substrates. Unexpectedly, no H-bonding interaction connecting the NO ligand to the active site water molecule or the Arg substrate was detected, in contrast to the results obtained by X-ray crystallography for the Arg-bound nNOS heme domain [Li et al. *J. Biol. Inorg. Chem*. **2006**, 11, 753–768]. The nearby exchangeable proton in both the no-substrate and Arg-containing nNOS samples is located outside the H-bonding range and, on the basis of the obtained structural constraints, can belong to the active site water (or OH). On the contrary, in the NOHA-bound sample, the nearby exchangeable hydrogen forms an H-bond with the NO ligand (on the basis of its distance from the NO ligand and a nonzero isotropic *hfi* constant), but it does not belong to the active site water molecule because the water oxygen atom (detected by $^{17}O$ ENDOR) is too far. This hydrogen should therefore come from the NOHA substrate, which is in

[*]**Corresponding Author:** Changjian Feng. Phone: 505-925-4326. Fax: 505-925-4549. cfeng@unm.edu.

**Supporting Information**

Local structures of the heme active sites of nNOS/Arg showing orientational heterogeneity of the NO ligand; numerical first derivatives of the field sweep ESE spectra; numerical simulation of the ESE field sweep spectrum of the impurity signal at $g = 2.027$; orientation-selective $^{1}H$ and $^{17}O$ ENDOR spectra; analysis of the $^{17}O$ ENDOR spectra; comparison between the nNOS/Arg $^{1}H$ ENDOR spectra at pH 6.0 and 7.4; preparation details of the nNOS/Arg sample at pH 6.0; Euler angles definition. The Supporting Information is available free of charge on the ACS Publications website at DOI: 10.1021/acs.jpca.5b01804.

**Notes**

The authors declare no competing financial interest.

agreement with the X-ray crystallography work [Li et al. *Biochemistry* **2009**, 48, 10246–10254]. The nearby nonexchangeable hydrogen atom assigned as $H_{\varepsilon}$ of Phe584 was detected in all three samples. This hydrogen atom may have a stabilizing effect on the NO ligand and probably determines its position.

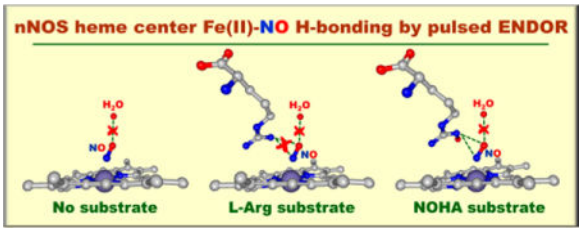


## INTRODUCTION

Mammalian nitric oxide synthases (NOSs) are enzymes responsible for oxidation of L-arginine (L-Arg) to nitric oxide (NO).[1] These reactions occur at the heme active site(s) in the oxygenase domain of NOS. Their mechanistic aspects are not completely understood,[2] and it is of current interest to study structures of the heme species that activates $O_2$ and transforms the substrate.[3] Knowledge of the relative structural arrangement of the heme, substrate, and possible other molecules relevant to catalysis is important for understanding the chemical mechanism. One specific, important problem is the role of hydrogen bonding, and in this context, of the active site water molecule, in the catalysis. According to the X-ray structures, a single water molecule is within H-bonding distance from the diatomic ligand ($O_2$) and is proposed to provide at least one of the protons necessary for promoting heterolytic cleavage of the O–O bond followed by oxidation of L-Arg to *N*-hydroxy-L-arginine (NOHA) and then to NO.[4]

Electron paramagnetic resonance (EPR) is a powerful tool for elucidating protein/enzyme structures both at the level of local environment of the enzyme active site(s)[5] and at the level of the overall protein geometry and folding (using site-directed spin labeling).[6] In addition to complementing X-ray crystallography by providing structural information in solution, EPR also can directly detect the presence of protons in the vicinity of a paramagnetic center. Importantly, it can determine if a hydrogen bond is formed between a particular hydrogen and the paramagnetic center.[7]

One of the most crucial and interesting paramagnetic intermediates in the catalytic NOS heme domain, the ferric (hydro)peroxo heme complex, is extremely reactive[8] and presents serious challenges for direct EPR detection. However, various indirect approaches to EPR investigations of the heme active site structure in this state can be employed. In some of the works by Brian Hoffman's group,[7b,9] the ferric intermediate was generated by using a cryoreduction technique. As a more accessible alternative, we have recently started pulsed EPR study of a stable ferrous nitrosyl form of NOS heme centers, which is isoelectronic to the native ferric (hydro)peroxo intermediate in NOS.[10] Another advantage of this approach is that a significant spin density is localized on the NO ligand, which improves EPR sensitivity to the structural details of the second coordination sphere.

Using this approach, we have previously obtained information on the position of the L-Arg substrate relative to the NO ligand of the ferrous–NO heme center of neuronal NOS (nNOS) and compared it with the crystal structure.[11] It was found that the L-Arg position in frozen solution is noticeably different from that in the crystal, with the shifts of some of the atoms as large as 1 Å. This result shows that although the crystal structures provide valuable guidance regarding the relative position of various structural elements of the protein and the substrate, a certain amount of caution should be exercised when these structures are used for making conclusions about possible interactions between the molecular components in solution. This is particularly significant in the case of the hydrogen bonding because a ~1 Å shift in the relative position of the potential hydrogen bonding partners may correspond to two qualitatively different chemical situations of the H-bond being either present or absent. In the present work, we used the pulsed electron–nuclear double resonance (ENDOR) at the microwave (mw) $K_a$ band (~30 GHz) to probe the hydrogen bonding of the NO ligand in the ferrous–NO nNOS samples without a substrate and with the L-Arg or NOHA substrate.

## MATERIALS AND METHODS

### 1. EPR Sample Preparation

Rat nNOS oxygenase (NOSoxy) construct, in which only the heme-containing oxygenase domain is present, was expressed and purified as reported earlier.[12] Three types of EPR samples were prepared in the $H_2O$, $D_2O$, or $H_2{}^{17}O$ buffers: without substrate, with L-Arg, or with NOHA. Buffer exchange into $D_2O$ was accomplished by concentrating the protein samples to 20 $\mu$L and then diluting to 0.5 mL with the appropriate Buffer in $D_2O$. This procedure was repeated three times. The value of pD was calculated as described by Glasoe and Long,[13] i.e., $pD_{true} = pD_{apparent} + 0.4$. The $^{17}O$-enrichment was accomplished by mixing the protein sample with 70% $H_2{}^{17}O$ buffer (final $H_2{}^{17}O$ concentration: ~50%). The EPR samples were then prepared in a septum-sealed quartz cuvette (Starna Cells, 9/Q/10-GL14-S). A 300 $\mu$L aliquot of 500 $\mu$M nNOSoxy was added into the cuvette; buffer: 100 mM Bis–Tris–propane, 200 mM NaCl, 1 mM DTT, 10 $\mu$M $H_4B$, 10% glycerol, pH 7.4. The protein solution was deoxygenated with three cycles of vacuum pumping and purging (with dioxygen-scrubbed argon gas). NO gas was introduced into the headspace until complete disappearance of the high spin ferric heme band at 650 nm, indicative of the formation of the ferric–NO adduct. The sample was then reduced with excess amount of freshly prepared dithionite solution. To prepare the substrate-containing samples, solid L-Arg hydrochloride or NOHA monoacetate salt was added to a final concentration of 10 mM; the change in pH of the sample was negligible. A ~45 $\mu$L sample was then transferred into an EPR tube and rapidly frozen in a pentane and liquid nitrogen slurry.

### 2. Pulsed EPR Experiments

The pulsed EPR experiments were performed on a home-built broadband (26–40 GHz) $K_a$-band pulsed EPR spectrometer.[14] The specific techniques used in this work to detect the $^{17}O$ and $^{1}H/^{2}H$ ENDOR spectra were the regular Mims ENDOR[15] and the refocused Mims ENDOR techniques,[7a,16] respectively. The detailed experimental conditions are given in the figure captions. The numerical simulations of the ENDOR spectra were performed using the SimBud software.[17]

# RESULTS AND DISCUSSION

## 1. Structural Background

In this work, we investigated the H-bonding of the NO ligand of the ferrous heme center of nNOS in the preparations without substrates and with L-Arg or NOHA substrate. For simplicity of reference, these respective samples are denoted nNOS/NS ("NS" stands for "No Substrate"), nNOS/Arg, and nNOS/NOHA. The relevant X-ray structures available in the protein data bank and described in the literature are those of the ferrous–NO form of the oxygenase domain of nNOS/Arg (pdb 2G6K) and nNOS/NOHA (pdb 3HSP). Figure 1 shows the relative positions of the NO-coordinated heme, the substrate, the oxygen of the active site water molecule, and the nearby amino acid residues implicated in the H-bonding with the active site water. The arrows in Figure 1 show the potential H-bonds between the active site water, substrate, and the NO ligand, as identified on the basis of the local geometric considerations in the X-ray investigations.[4] To the best of our knowledge, no X-ray structures for the ferrous–NO form of the oxygenase domain of nNOS/NS are available.

## 2. Approach and Complications

To detect the H-bonding of the NO ligand, $^{1}H$, $^{2}H$, and $^{17}O$ ENDOR experiments were performed with the samples prepared in $H_2O$, $D_2O$, and $H_2{}^{17}O$. The $^{2}H$ ENDOR and the "$H_2O$ – $D_2O$" difference $^{1}H$ ENDOR spectra show the deuterons and the exchangeable protons, respectively. The distances from the NO ligand to the exchangeable protons are estimated from the anisotropic *hfi* that is found from the analysis of the ENDOR spectra. These distances represent the basis for making a decision regarding possible H-bonding. To qualify as H-bonds, these distances should be smaller than the sum of the van der Waals radii of N or O, ~1.55 and 1.52 Å, respectively, and H, ~1.2 Å. In addition, a nonzero isotropic *hfi* constant is expected in the case of an H-bond. The $^{17}O$ spectra mostly play an auxiliary role: they help to establish if the H-bonded hydrogen(s) could belong to the nearby active site water.

To estimate the distance from the NO ligand to a particular proton (or another magnetic nucleus) from its *hfi* anisotropy, one must take into account the distribution of the electronic spin density over the Fe–NO fragment. Several distributions were estimated by density functional theory (DFT) calculations[7c,d,18] ranging from ($\rho_{Fe}$, $\rho_{NO}$) ≈ (0.74, 0.26) to (−0.2, +1.2). The analysis of the ENDOR spectra from L-Arg substrate enriched in $^{2}H$ at carbon positions and $^{15}N$ at guanidino nitrogens in our previous work[11] has shown that the intermediate spin population distribution with ($\rho_{Fe}$, $\rho_{NO}$) ≈ (0.2, 0.8) predicted in some of the DFT studies[18b,c,19] is the most realistic one, and we will continue using such a distribution in this work. The relative spin populations on N and O were found to be about 1:0.6,[20] which results in the absolute spin populations of $\rho_N = 0.5$ and $\rho_O = 0.3$.

The second complication arises from the fact that at least in some of the X-ray structures of NOS oxygenase domain the orientations of the NO ligand for the two heme sites, A and B, are noticeably different (Figure S1, Supporting Information).[4b] This could present problems with interpreting the EPR data if NO orientational heterogeneity also is present in frozen solution. In our previous work,[11] we have shown that in the case of such orientation

differences, the magnitudes of the anisotropic *hfi* tensor components are affected significantly less (in fact, they are nearly invariant at sufficiently large distances) than the orientations of the *hfi* tensors with respect to the *g*-frame, which is linked to the NO-ligand orientation. This conclusion is also supported by the anisotropic *hfi* values calculated for the relevant magnetic nuclei using the crystal structures (Table 1). The possible orientational inhomogeneity of the *hfi* tensors makes the analysis of the orientation-selective ENDOR spectra extremely difficult, especially taking into account the fact that they are contributed to by multiple nuclei. To simplify the data interpretation, similar to our previous work,[11] we used in our analysis the field-integrated (FI) ENDOR spectra[21] obtained as weighted sums of the normalized (by the ESE amplitude without RF) orientation-selective spectra aligned at the Zeeman frequency of the nucleus of interest (in this work, $^{1}$H or $^{17}$O), with the statistical weights given by the relative amplitudes of the ESE signal at the corresponding measurement positions (i.e., $p_k = A_k/\Sigma_j A_j$, where $p_k$ is the statistical weight of the $k$th orientation-selective ENDOR spectrum and $A_i$ are the field-sweep ESE spectrum amplitudes at the ENDOR measurement positions). The FI spectra represent an approximation to the spectra that would be obtained in the orientationally nonselective situation (in this case, for the hypothetical situation of isotropic *g*-factor of Fe(II)–NO center).

## 3. Field Sweep Spectra

Figure 2 shows the electron spin echo (ESE) field sweep spectra obtained at the mw $K_a$ band (~30 GHz) for the samples of nNOS/NS, nNOS/Arg, and nNOS/NOHA (numerical first derivatives of these spectra are shown in Figure S2 of the Supporting Information). One can see that the spectra of nNOS/NS and nNOS/Arg are nearly identical and exhibit a resolved triplet structure at the intermediate turning point, $g_Y$, due to the *hfi* of the $^{14}$N nucleus that belongs to the NO ligand ($A_Y \approx 2.1$ mT). The spectrum of nNOS/NOHA is very different, with smaller overall *g*-anisotropy, but significantly greater g-strain broadening, which obliterates the hyperfine structure at $g_Y$.

The principal *g*-values determined from these spectra are $(g_X, g_Y, g_Z) \approx (1.969, 2.003, 2.083)$ for nNOS/NS, $(g_X, g_Y, g_Z) \approx (1.969, 2.003, 2.084)$ for nNOS/Arg, and $(g_X, g_Y, g_Z) \approx (1.985, 2.007, 2.076)$ for nNOS/NOHA. These principal *g*-values are mostly in good agreement with those determined by continuous wave EPR at the X-band.[10b] The only notable difference is the intermediate *g*-value of nNOS/NOHA, 2.007 in this work vs 2.021 estimated at X-band. The value found in this work is more accurate because the assignment of the EPR turning points at $K_a$-band is straightforward due to a higher Zeeman resolution, whereas at the X-band the $g_Y$ region of the spectrum is complicated, making a definitive assignment difficult.[10b]

The feature marked by an asterisk is located at $g \approx 2.027$. It is the largest in the spectrum of nNOS/NOHA, but in the other two spectra it is also present, although with a smaller amplitude. This feature was observed in ferrous–NO samples of various heme proteins,[7c,d,22] and its origin is not entirely clear. The DFT calculations suggest that it could result from a 5-coordinate heme with the NO ligand in an eclipsed conformation, i.e., when the Fe–NO plane (approximately) coincides with the $N_{(NO)}$–Fe–$N_{(porph)}$ plane.[18a] This would indicate that in a minor fraction of the nNOS heme sites the cysteine ligand could

have (partially) dissociated. A numerical simulation (Figures S2 and S3, Supporting Information) shows that the contribution of this species to the ESE signal for nNOS/NOHA sample does not exceed 15%. Therefore, regardless of the origin, such a minor species does not interfere with the analysis of the ENDOR data, where only major ENDOR lines are considered.

## 4. ENDOR Spectra of Nonexchangeable Protons

Figure 3 shows the ENDOR spectra of nonexchangeable protons obtained at the EPR positions where the largest splitting between the ENDOR lines is observed (see Figure S4 of Supporting Information for the full set of the orientation-selective spectra). The largest splitting is achieved at the EPR position approximately 13 mT (for nNOS/NS and nNOS/Arg) or 11 mT (nNOS/NOHA) downfield from $g_Y$, and it equals to about 7.65 MHz. Assuming the isotropic *hfi* constant, $a_{iso}$, to be zero, which is reasonable for nonexchangeable protons, one can equate this splitting with the largest component of the anisotropic *hfi* tensor, $T_{||}$ (in spite of a possibility of some nonaxiality of the *hfi* tensor, we will still retain the notation $T_{||}$ for this component). This EPR position corresponds to the angle between the axis of $g_Z$ and the vector of the external magnetic field, $B_o$, of $\theta_B \approx 52° \pm 6°$ (depending on the azimuthal angle of $B_o$ in the *g*-frame).

To obtain structural information for a magnetic nucleus (proton or $^{17}O$) from its anisotropic *hfi*, the following approach was used. The possible positions of the nucleus with respect to the NO ligand were calculated using the three-point spin density distribution ($\rho_{Fe}$, $\rho_N$, $\rho_O$) = (0.2, 0.5, 0.3) described above. Specifically, the anisotropic *hfi* tensor was calculated for a trial position of the magnetic nucleus, and this position was varied until the agreement with the experimental $T_{||}$ value was reached. For any given $T_{||}$ value, the solution is not unique, and the whole set of solutions represents a surface enveloping the Fe–NO fragment.

Because $\rho_{Fe}$ is small, the solution surface has a near-cylindrical symmetry with respect to the N–O bond in the part of space distant from the Fe(II) ion (i.e., where the studied second sphere nuclei are located). For this part of space, the obtained possible positions for a given magnetic nucleus can be presented by a line in the *XY* coordinate system with axis *X* coinciding with the N–O bond and the nitrogen atom located at the coordinate origin. This line represents an intersection of the solution surface with the *XY* plane. The direction of axis *Y* is generally different for each magnetic nucleus: it is selected in such a way that this nucleus is located in the (++) quadrant of the *XY* plane. As a consequence of the near-cylindrical symmetry, the 2D position estimates virtually do not depend on the specific orientation of axis *Y* as long as it points in a general direction parallel to or away from the heme plane and the heme Fe atom. Such a flexible definition of the *Y* axis allows one to conveniently present the positions of all relevant surrounding magnetic nuclei on the *XY* plane. The above description of the *XY* coordinate system implies that the Fe(II) ion, which is not explicitly shown in the plots, is located at $X_{Fe} \approx -1.53$ Å and $Y_{Fe} \in [-0.92, 0]$ Å, depending on specific orientation of the *Y*-axis. Such *XY* coordinate system is used in Figures 4 and 6 below.

The calculated range of possible positions of the nonexchangeable proton with $T_{||} = 7.65$ MHz is shown by the solid black line in Figure 4. The analysis of the X-ray structures shows

that the closest proton to the NO ligand is $H_\varepsilon$ of Phe 584 (Figure S1 of the Supporting Information). The positions of this proton obtained from several X-ray structures are shown by black open circles. Good agreement between the X-ray and ENDOR distances in this case provides extra support to the spin density distribution ($\rho_{Fe}$, $\rho_N$, $\rho_O$) = (0.2, 0.5, 0.3) used in our distance calculations.

The angles $\theta_B$ calculated for $H_\varepsilon$ of Phe 584 using the X-ray structures of nNOS/Arg and nNOS/NOHA are within the range of 50–56°, in agreement with the experimental ENDOR observations. In these estimates, the *g*-tensor orientation established both by DFT calculations and by X-ray crystallography for the 6-coordinated ferrous–NO heme centers[4] was used, with the axis of $g_Z$ lying in the heme plane, perpendicular to the Fe–NO plane, and the axis of $g_X$ approximately coinciding with the direction of the NO bond.

## 5. ENDOR Spectra of Exchangeable Protons

Figure 5 shows the FI $^1$H ENDOR spectra obtained as a difference between those recorded for the samples prepared in $H_2O$ and $D_2O$ (the original orientation-selective spectra used to calculate the FI spectra are shown in Figure S4 of the Supporting Information). The difference spectra of nNOS/NS and nNOS/Arg are significantly narrower than that of nNOS/NOHA. The numerical simulations of the spectra (dashed lines in Figure 5) show that while in the first two cases the *hfi* is purely anisotropic ($a_{iso}$ = 0), in the last case a noticeable isotropic *hfi* constant is present ($a_{iso} \approx -0.6$ MHz). The anisotropic *hfi* in the cases of nNOS/NS and nNOS/Arg is with good accuracy axial, with $T_{||}$ about 3 MHz. In the case of nNOS/NOHA, the anisotropic *hfi* is noticeably rhombic and is about twice as strong: $T_{||} \approx 5.7$ MHz.

The solid black lines in Figure 6 show the possible positions of the nearby exchangeable protons with respect to the NO ligand calculated on the basis of the $T_{||}$ values obtained from ENDOR and using ($\rho_{Fe}$, $\rho_N$, $\rho_O$) = (0.2, 0.5, 0.3). The shaded area indicates the H-bonding distance range defined as the sum of the van der Waals radii of H and N or O. One can see that for the nNOS/NS and nNOS/Arg samples the nearby exchangeable proton is outside the H-bonding range, whereas in the case of NOHA it is within the H-bonding range. A weak H-bond with NOHA is consistent with the nonzero isotropic *hfi* constant ($a_{iso} \approx -0.6$ MHz; see above). The assignment of the H-bonding hydrogen in the nNOS/NOHA sample is discussed below.

## 6. $^{17}$O ENDOR Spectra

Figure 7 shows the $^{17}$O FI ENDOR spectra obtained for samples prepared with $^{17}$O-enriched water (solid lines; the original orientation-selective spectra used to calculate the FI spectra are shown in Figure S5 of the Supporting Information). These spectra exhibit two distinct features: the relatively narrow central peak due to the +1/2 ↔ −1/2 transition of $^{17}$O (the noticeable asymmetry of this peak is caused by the second order effects of the *nqi*) and a broad background peak mostly contributed to by ±1/2 ↔ ±3/2 transitions. The lines of ±3/2 ↔ ±5/2 transitions are about twice as broad and about one-half in amplitude. Our approach to the numerical simulations of these spectra is described in the Supporting Information. The results of the simulations are shown by the dashed lines in Figure 7. In contrast to the

exchangeable protons results (see the anisotropic *hfi* values above), the weakest $^{17}O$ *hfi* is observed for nNOS/NOHA ($T_{||}$ = −0.23 ± 0.02 MHz), whereas the strongest one is found for the nNOS/NS sample ($T_{||}$ = −0.36 ± 0.05 MHz).

The red lines in Figure 6 show the possible positions of the active site water oxygen for each of the samples obtained from the analysis of the $^{17}O$ anisotropic *hfi*. One can see that for the nNOS/NS and nNOS/Arg samples the minimal projection of the distance between the nearby exchangeable proton and the $^{17}O$ on the *XY* plane of the figure is shorter than the OH bond length of ~1 Å. This indicates that the nearby exchangeable proton detected by ENDOR can belong to the active site water molecule. In contrast, the projection of the H–O distance on the *XY* plane in the case of nNOS/NOHA is at least 1.4 Å, significantly greater than the OH bond length. It thus follows that the nearby exchangeable proton in nNOS/NOHA cannot belong to the active site water molecule. The most likely other H-bonding candidate in this case is the NH hydrogen of NOHA, as suggested in the X-ray crystallographic work.[4a]

## 7. Comparison with the Crystal Structures

The red open circles in Figure 6 indicate the positions of the active site water oxygen atom in the crystal structures of nNOS/Arg and nNOS/NOHA (for nNOS/NS no X-ray data are available). The ~3 Å distance between this oxygen atom and the NO ligand observed in the crystal structures was interpreted as pointing at the existence of a hydrogen bond between these two moieties, at least in nNOS/Arg (for nNOS/NOHA, the water molecule was suggested to be an H-bond donor to the nitrogen of the NH–OH group of NOHA; see Figure 1B).[4b] The positions of the water hydrogen in the nNOS/Arg active sites predicted from the crystallographic positions of the water oxygen in the heme sites A and B are shown by black open circles in the middle panel of Figure 6.

Although the water oxygen positions estimated by ENDOR are at least 0.5 Å longer than those obtained by X-ray crystallography, they formally allow a similar interpretation in terms of potential H-bonding with the NO ligand. For instance, using the $^{17}O$ position obtained by ENDOR for nNOS/Arg, one could place the water hydrogen marginally within the H-bonding distance range: at least for the $O_{NO}$–$N_{NO}$–Owater angles under 30°, the $O_{NO}$–H distance predicted from the $^{17}O$ position would be ~2.5–2.6 Å. The latter distance could even be shortened to ~2.4 Å by considering a stronger $^{17}O$ anisotropic *hfi* at the margin of the error limits (−0.3 Å rather than the median value of −0.27 Å). Fortunately, however, with the magnetic resonance approach one does not need to make such predictions because the protons (unlike in the X-ray crystallography) are observable directly and the distances to them are readily obtained from the analysis of the $^{1}H$ ENDOR data. This direct estimate (solid black line in Figure 6) places the nearby exchangeable proton in nNOS/Arg outside the H-bonding range.

Thus, although both the X-ray and ENDOR water oxygen positions in nNOS/Arg are formally within the H-bonding range from the NO ligand, the $^{1}H$ ENDOR data for the frozen solution sample show definitively that the exchangeable protons are outside the H-bonding range. It is not clear, however, if the latter observation reflects an actual difference with the situation in a crystal sample studied by the X-ray crystallography because the

hydrogen atoms are not directly observed by the X-ray, and it may be difficult to unequivocally assign the actual H-bond partner(s) on the basis ofly on the positions of heavier atoms such as oxygen.

For nNOS/NOHA, the situation is different. Although we found the water oxygen to be at least 0.5 Å further away from the NO ligand than in the X-ray structure, the ENDOR estimate for the nearby exchangeable proton position is in good agreement with the predicted position of the NH hydrogen atom of NOHA (black open circles in the bottom panel of Figure 6). The nearby hydrogen atom forms an H-bond with the NO ligand, in agreement with the conclusions of the X-ray crystallographic work.[4a]

To improve the agreement between the X-ray and ENDOR $O_{water}$ positions, we have made an attempt to reconsider the spin density distribution in the Fe–N–O fragment of the heme center. As stated above, the ENDOR data were analyzed in terms of structure using ($\rho_{Fe}$, $\rho_N$, $\rho_O$) = (0.2, 0.5, 0.3). The fact that the ENDOR distances estimated using these spin densities are significantly larger than those found in the crystal structures could be interpreted as implying that $\rho_N$ and $\rho_O$ are actually smaller than those we used. The analysis of all available data (both obtained here and in our earlier work[11]) shows, however, that no satisfactory solution for this problem exists. For example, the spin density distribution required to match the ENDOR estimate of the water oxygen position in nNOS/Arg ($T_{||}$ = −0.27 MHz) with that obtained by X-ray is ($\rho_{Fe}$, $\rho_N$, $\rho_O$) ≈ (0.65, 0.22, 0.13) (assuming $\rho_O/\rho_N$ = 0.6, as discussed above). Such a distribution, however, will place the guanidino nitrogen of the L-Arg substrate ($T_{||}$ = 0.66 MHz for $^{14}N$) at 1.8 Å from N(NO), which is approaching a covalent bonding distance (1.4–1.45 Å) and is therefore completely unrealistic. This distance is also significantly shorter than the X-ray crystallographic distance of about 3 Å. The $H_\varepsilon$ proton of Phe 586 will be located at the estimated 1.65 Å from O(NO), also noticeably closer than the X-ray distance of 2.2 Å.

In the distribution discussed above, the overall spin density on the NO ligand was reduced in favor of the central Fe ion, but the ratio of $\rho_O/\rho_N$ = 0.6 was retained. Alternatively, one can keep $\rho_N + \rho_O$ = 0.8 constant but increase $\rho_N$ at the expense of $\rho_O$. Because the water oxygen is closer to O(NO) than to N(NO) (on the basis of the crystal structures), this might also make the ENDOR estimates for $^{17}O$ more similar to the X-ray distance. Dashed lines in Figures 4 and 6 show, as an example, the calculated possible positions for ($\rho_{Fe}$, $\rho_N$, $\rho_O$) = (0.2, 0.7, 0.1), where most of the spin density is concentrated on the NO ligand nitrogen. Even such an extreme and totally unrealistic distribution, however, does not result in agreement between the ENDOR and X-ray oxygen positions. It also does not change our conclusions regarding the H-bonding situation because the closest possible positions the exchangeable proton in nNOS/NS and nNOS/Arg are on the border or barely within the formal H-bonding range (see the dashed lines in Figure 6).

We therefore confirm the conclusion of our previous work that the spin density distribution of ~ (0.2, 0.5, 0.3) produces the most balanced results and is the most realistic one. Two kinds of reasons may be responsible for the deviations from the X-ray data. First, the changes could be attributed to the fact that the crystals for the X-ray investigation were grown from solutions at pH 5.6–6.0,[4b] whereas our solution samples were prepared at pH

7.4. It is conceivable that the increase in pH could lead to minor nonspecific structural alterations. It could also result in the active site water molecule being replaced by a hydroxide, $HO^-$, which could dramatically change the hydrogen bonding situation at the heme active site. To test the potential effect of pH, we investigated a sample of nNOS/Arg at pH 6.0. The EPR and ENDOR spectra for this sample were identical to those of the sample prepared at pH 7.4 (Figure S8, Supporting Information). The effect of pH can thus be excluded from consideration.

Alternatively, the differences could be caused by structural restrictions imposed by the crystal packing, which are absent for the protein in solution. A certain degree of inherent structural flexibility in the side chains could lead to subtle structural rearrangements (note that the absolute differences of the relevant distances are on the order of 1 Å) compared to the crystal structure. This implies, in particular, that in liquid solution the hydrogen bonding network at the heme active site is most likely dynamic, with the H-bonds forming, breaking, and switching between various partners in response to the relatively minor modifications of the local protein geometry. In some structural realizations (e.g., nNOS in a crystal[4b]), the H-bond between the active site water and the NO ligand (or, the peroxo ligand in the case of ferric peroxo intermediate) required by the NOS mechanism is formed. In other structural realizations (like that observed in this work for nNOS/NS or nNOS/Arg in frozen solution), the NO ligand does not participate in the hydrogen bonding.

This dynamic model allows one to reconcile the absence of any H-bonding to the NO ligand in the nNOS/Arg sample (as observed in this work by pulsed ENDOR) with the proton availability (supposedly provided by the H-bonding) necessary for the cleavage of the O–O bond and subsequent hydroxylation of L-Arg to NOHA;[4b,23] note that the NOS ferrous–NO complex is a close mimic of the obligatory ferric (hydro)peroxo intermediate in NOS catalysis.[10] An attractive feature of this model is that it naturally allows the ligand, water, and substrate molecules to be readily incorporated into or released from the active site. An additional observation in support of this view is that in the Enos–NO structure[24] the electron density for the water molecule near the NO ligand is weak even though the amino acids and the local protein structures surrounding the NO ligand are identical in eNOS[24] and nNOS.[4b] Thus, the two crystal structures (nNOS and eNOS) represent the two extremes, ordered water and weakly bound water in the active site, whereas our present results provide a picture midway between these two extremes.

With this dynamic model, it is reasonable to expect that the specific H-bonding situation observed for a given NOS sample might depend on the NOS isoform, substrate, and the type of the heme complex. Indeed, the H-bonding situation for the nNOS/NOHA sample observed in this work is qualitatively similar to that in a crystal structure.[4a] Another example is provided by the study of peroxoferri–NOS form in the cryo-reduced oxy–eNOS with Arg substrate, where a proton characterized by significant anisotropic and isotropic *hfi* (signifying the H-bond formation) was detected by $^1$H ENDOR in the frozen solution sample, which was prepared at pH 7.4.[7b]

It is also interesting to note that there is a correlation between the ENDOR structural results and the shape of the EPR spectra. The EPR spectra of nNOS/NS and nNOS/Arg are nearly

identical, which correlates with the fact that in both preparations the NO ligand does not form hydrogen bonds with either water oxygen or the guanidino nitrogen of L-Arg substrate. In nNOS/NOHA, on the contrary, the NO ligand forms a hydrogen bond with the substrate (NOHA), which possibly results in a slight repositioning of this ligand and, as a consequence, in the change of the EPR spectrum (interestingly, the rhombic form of the EPR spectrum of myoglobin–NO, where the NO ligand participates in an H-bonding, has the principal g-values similar to those of nNOS/NOHA[7c]). A minor redistribution of the electronic and spin density in the Fe–NO fragment caused by the H-bond could also contribute to the observed change of the EPR spectrum.

The nearby nonexchangeable hydrogen atom assigned as $H_{\varepsilon}$ of Phe584 was detected in all three samples. This hydrogen atom may have a stabilizing effect on the NO ligand and probably determines its position: $H_{\varepsilon}$ eclipses one of $C_{meso}$ atoms of the heme, whereas the oxygen of NO eclipses a pyrrole nitrogen on either side of that $C_{meso}$ (Figure S1, Supporting Information). On the basis of the NO–$H_{\varepsilon}$ distance of about 2.2 Å, it appears that there should be some specific interaction between the NO and $H_{\varepsilon}$. Although the H-bond with a C–H hydrogen is traditionally believed impossible (because the CH bond is practically nonpolar), the existence of such bonds has been considered in the literature already for several decades, and lately such a concept was employed to explain protein structures.[25] One may speculate that such a specific interaction with $H_{\varepsilon}$ of Phe584 also exists in the native ferric–$O_2$ complex (the analog of which ferrous–NO represents), and it plays a role in positioning the peroxide ligand properly for the interaction with the substrate.

## CONCLUSION

This investigation aimed to obtain direct information about the H-bonding network at the heme active site(s) of nNOS using the ferrous–NO mimic of the ferri–peroxo species. Unexpectedly, however, no H-bonding interactions connecting the NO ligand to the active site water molecule or Arg substrate were detected, in contrast to the results obtained earlier by X-ray crystallography for nNOSoxy containing the Arg substrate.[4b] The nearby exchangeable proton in both the nNOS/NS and nNOS/Arg samples is located outside the H-bonding range and, on the basis of the obtained structural constraints, can belong to the active site water (or OH). On the contrary, in the NOHA-bound sample, the nearby exchangeable hydrogen forms an H-bond with the NO ligand (on the basis of its distance from the NO ligand and a nonzero isotropic *hfi* constant), but it does not belong to the active site water molecule because the water oxygen atom (detected by $^{17}O$ ENDOR) is too far. This hydrogen should therefore come from the NOHA substrate, which is in agreement with the X-ray work.[4a]

The apparent contradiction between the lack of any H-bonding as observed for the NO ligand in nNOS/Arg by $^{1}H$ pulsed ENDOR in this work and the necessity of such H-bonding for the hydroxylation of L-Arg to NOHA is rationalized by hypothesizing that in liquid solution the H-bonding network at the heme active site is most likely dynamic, with various transient H-bonds being formed in response to the relatively minor modifications of the local protein geometry. The specific H-bonding situations observed in the crystal (where the H-bond with the NO ligand is likely present) and in frozen solution (no H-bond with the NO

ligand) correspond to somewhat different local structural realizations stabilized in these samples and are within the overall range of possible H-bonding situations realized in a liquid solution.

## Supplementary Material

Refer to Web version on PubMed Central for supplementary material.

## Acknowledgments

This work was supported by NIH GM081811 to C.F., NSF CHE-1150644 to C.F., AHA Grant-in-Aid 12GRNT11780019 to C.F., NIH GM57353 to T.L.P., and NIH GM052419 to L.J.R. A.V.A. gratefully acknowledges the NSF (DBI-0139459, DBI-9604939, BIR-9224431) and NIH (S10RR020959, 1S10RR026416-01) grants for the development of the EPR facility at the University of Arizona.

## References

1. Alderton WK, Cooper CE, Knowles RG. Nitric Oxide Synthases: Structure Function and Inhibition. Biochem J. 2001; 357:593–615. [PubMed: 11463332]
2. (a) Woodward JJ, Chang MM, Martin NI, Marletta MA. The Second Step of the Nitric Oxide Synthase Reaction: Evidence for Ferric-Peroxo as the Active Oxidant. J Am Chem Soc. 2009; 131(1):297–305. [PubMed: 19128180] (b) Zhu Y, Silverman RB. Revisiting Heme Mechanisms. A Perspective on the Mechanisms of Nitric Oxide Synthase (NOS), Heme Oxygenase (HO), and Cytochrome P450s (Cyp450s). Biochemistry. 2008; 47(8):2231–2243. [PubMed: 18237198]
3. (a) Hannibal L, Page RC, Haque MM, Bolisetty K, Yu Z, Misra S, Stuehr DJ. Dissecting Structural and Electronic Effects in Inducible Nitric Oxide Synthase. Biochem J. 2015; 467(1):153–65. [PubMed: 25608846] (b) Crane BR, Sudhamsu J, Patel BA. Bacterial Nitric Oxide Synthases. Annu Rev Biochem. 2010; 79(1):445–470. [PubMed: 20370423] (c) Santolini J. The Molecular Mechanism of Mammalian NO-Synthases: A Story of Electrons and Protons. J Inorg Biochem. 2011; 105(2):127–141. [PubMed: 21194610]
4. (a) Doukov T, Li HY, Soltis M, Poulos TL. Single Crystal Structural and Absorption Spectral Characterizations of Nitric Oxide Synthase Complexed with $N^{(\omega)}$-Hydroxy-L-Arginine and Diatomic Ligands. Biochemistry. 2009; 48(43):10246–10254. [PubMed: 19791770] (b) Li HY, Igarashi J, Jamal J, Yang WP, Poulos TL. Structural Studies of Constitutive Nitric Oxide Synthases with Diatomic Ligands Bound. JBIC J Biol Inorg Chem. 2006; 11(6):753–768. [PubMed: 16804678]
5. Hoffman BM. Electron-Nuclear Double Resonance Spectroscopy (and Electron Spin-Echo Envelope Modulation Spectroscopy) in Bioinorganic Chemistry. Proc Natl Acad Sci U S A. 2003; 100(7):3575–3578. [PubMed: 12642664]
6. de Vera, IMS.; Blackburn, ME.; Galiano, L.; Fanucci, GE. Current Protocols in Protein Science. John Wiley & Sons, Inc; New York: 2013. Pulsed EPR Distance Measurements in Soluble Proteins by Site-Directed Spin Labeling (SDSL).
7. (a) Astashkin AV, Kawamori A, Kodera Y, Kuroiwa S, Akabori K. An Electron Spin Echo Envelope Modulation Study of the Primary Acceptor Quinone in Zn-Substituted Plant Photosystem II. J Chem Phys. 1995; 102(14):5583–5588.(b) Davydov R, Ledbetter-Rogers A, Martasek P, Larukhin M, Sono M, Dawson JH, Masters BSS, Hoffman BM. EPR and ENDOR Characterization of Intermediates in the Cryoreduced Oxy-Nitric Oxide Synthase Heme Domain with Bound L-Arginine or N-G-Hydroxyarginine. Biochemistry. 2002; 41(33):10375–10381. [PubMed: 12173923] (c) Radoul M, Sundararajan M, Potapov A, Riplinger C, Neese F, Goldfarb D. Revisiting the Nitrosyl Complex of Myoglobin by High-Field Pulse EPR Spectroscopy and Quantum Mechanical Calculations. Phys Chem Chem Phys. 2010; 12(26):7276–7289. [PubMed: 20490401] (d) Radoul M, Bykov D, Rinaldo S, Cutruzzolà F, Neese F, Goldfarb D. Dynamic Hydrogen-Bonding Network in the Distal Pocket of the Nitrosyl Complex of *Pseudomonas Aeruginosa* $cd_1$ Nitrite Reductase. J Am Chem Soc. 2011; 133(9):3043–3055. [PubMed: 21309511]

8. Davydov R, Sudhamsu J, Lees NS, Crane BR, Hoffman BM. EPR and ENDOR Characterization of the Reactive Intermediates in the Generation of NO by Cryoreduced Oxy-Nitric Oxide Synthase from Geobacillus Stearothermophilus. J Am Chem Soc. 2009; 131(40):14493–14507. [PubMed: 19754116]
9. Davydov R, Labby KJ, Chobot SE, Lukoyanov DA, Crane BR, Silverman RB, Hoffman BM. Enzymatic Cryoreduction and EPR Studies of the Hydroxylation of Methylated $N^{\omega}$-Hydroxy-L-Arginine Analogues by Nitric Oxide Synthase from Geobacillus Stearothermophilus. Biochemistry. 2014; 53(41):6511–6519. [PubMed: 25251261]
10. (a) Couture M, Adak S, Stuehr DJ, Rousseau DL. Regulation of the Properties of the Heme-NO Complexes in Nitric-Oxide Synthase by Hydrogen Bonding to the Proximal Cysteine. J Biol Chem. 2001; 276(41):38280–38288. [PubMed: 11479310] (b) Migita CT, Salerno JC, Masters BSS, Martasek P, McMillan K, IkedaSaito M. Substrate Binding-Induced Changes in the EPR Spectra of the Ferrous Nitric Oxide Complexes of Neuronal Nitric Oxide Synthase. Biochemistry. 1997; 36(36):10987–10992. [PubMed: 9283090]
11. Astashkin AV, Elmore BO, Chen L, Fan W, Guillemette JG, Feng C. Pulsed ENDOR Determination of the Arginine Location in the Ferrous–NO Form of Neuronal NOS. J Phys Chem A. 2012; 116(25):6731–6739. [PubMed: 22667467]
12. (a) Feng CJ, Tollin G, Hazzard JT, Nahm NJ, Guillemette JG, Salerno JC, Ghosh DK. Direct Measurement by Laser Flash Photolysis of Intraprotein Electron Transfer in a Rat Neuronal Nitric Oxide Synthase. J Am Chem Soc. 2007; 129(17):5621–5629. [PubMed: 17425311] (b) Ghosh DK, Holliday MA, Thomas C, Weinberg JB, Smith SME, Salerno JC. Nitric-Oxide Synthase Output State - Design and Properties of Nitric-Oxide Synthase Oxygenase/FMN Domain Constructs. J Biol Chem. 2006; 281(20):14173–14183. [PubMed: 16461329] (c) Ghosh DK, Wu CQ, Pitters E, Moloney M, Werner ER, Mayer B, Stuehr DJ. Characterization of the Inducible Nitric Oxide Synthase Oxygenase Domain Identifies a 49 Amino Acid Segment Required for Subunit Dimerization and Tetrahydrobiopterin Interaction. Biochemistry. 1997; 36(35):10609–10619. [PubMed: 9271491]
13. Glasoe PK, Long FA. Use of Glass Electrodes to Measure Acidities in Deuterium Oxide. J Phys Chem. 1960; 64(1):188–190.
14. Astashkin AV, Enemark JH, Raitsimring A. 26.5–40 GHz $K_a$-band Pulsed EPR Spectrometer. Concepts Magn Reson, Part B. 2006; 29B(3):125–136.
15. Mims WB. Pulsed ENDOR Experiments. Proc R Soc London, Ser A. 1965; 283(1395):452–457.
16. Doan PE, Hoffman BM. Making Hyperfine Selection in Mims ENDOR Independent of Deadtime. Chem Phys Lett. 1997; 269(3–4):208–214.
17. Astashkin, AV. Simbud. http://www.cbc.arizona.edu/facilities/epr_facility_software.
18. (a) Patchkovskii S, Ziegler T. Structural Origin of Two Paramagnetic Species in Six-Coordinated Nitrosoiron(II) Porphyrins Revealed by Density Functional Theory Analysis of the G Tensors. Inorg Chem. 2000; 39(23):5354–5364. [PubMed: 11154592] (b) Praneeth VKK, Neese F, Lehnert N. Spin Density Distribution in Five- and Six-Coordinate Iron(II)–Porphyrin NO Complexes Evidenced by Magnetic Circular Dichroism Spectroscopy. Inorg Chem. 2005; 44(8):2570–2572. [PubMed: 15819537] (c) Praneeth VKK, Haupt E, Lehnert N. Thiolate Coordination to Fe(II)-Porphyrin NO Centers. J Inorg Biochem. 2005; 99(4):940–948. [PubMed: 15811511]
19. Praneeth VKK, Näther C, Peters G, Lehnert N. Spectroscopic Properties and Electronic Structure of Five- and Six-Coordinate Iron(II) Porphyrin NO Complexes: Effect of the Axial N-Donor Ligand. Inorg Chem. 2006; 45(7):2795–2811. [PubMed: 16562937]
20. Lehnert N. The spin populations of N and O predicted by DFT are about 0.5 and 0.3, respectively. Private communication.
21. (a) Astashkin AV, Klein EL, Enemark JH. Toward Modeling the High Chloride, Low pH Form of Sulfite Oxidase: $K_a$-band ESEEM of Equatorial Chloro Ligands in Oxomolybdenum(V) Complexes. J Inorg Biochem. 2007; 101(11–12):1623–1629. [PubMed: 17644181] (b) Astashkin AV, Johnson-Winters K, Klein EL, Byrne RS, Hille R, Raitsimring AM, Enemark JH. Direct Demonstration of the Presence of Coordinated Sulfate in the Reaction Pathway of *Arabidopsis Thaliana* Sulfite Oxidase Using $^{33}S$ Labeling and ESEEM Spectroscopy. J Am Chem Soc. 2007; 129(47):14800–14810. [PubMed: 17983221]

22. (a) O'Keeffe DH, Ebel RE, Peterson JA. Studies of the Oxygen Binding Site of Cytochrome P-450. Nitric Oxide as a Spin-Label Probe. J Biol Chem. 1978; 253(10):3509–3516. [PubMed: 206545] (b) Tsubaki M, Hiwatashi A, Ichikawa Y, Hori H. Electron Paramagnetic Resonance Study of Ferrous Cytochrome P-450scc-Nitric Oxide Complexes: Effects of Cholesterol and Its Analogs. Biochemistry. 1987; 26(14):4527–4534. [PubMed: 2822097]

23. Li D, Kabir M, Stuehr DJ, Rousseau DL, Yeh SR. Substrate- and Isoform-Specific Dioxygen Complexes of Nitric Oxide Synthase. J Am Chem Soc. 2007; 129(21):6943–6951. [PubMed: 17488012]

24. Li HY, Raman CS, Martasek P, Masters BSS, Poulos TL. Crystallographic Studies on Endothelial Nitric Oxide Synthase Complexed with Nitric Oxide and Mechanism-Based Inhibitors. Biochemistry. 2001; 40(18):5399–5406. [PubMed: 11331003]

25. (a) Brandl M, Lindauer K, Meyer M, SüChnel J. C–H···O and C–H···N Interactions in RNA Structures. Theor Chem Acc. 1999; 101(1–3):103–113.(b) Sarkhel S, Desiraju GR. N-H···O, O-H···O and C-H···O Hydrogen Bonds in Protein–Ligand Complexes: Strong and Weak Interactions in Molecular Recognition. Proteins: Struct, Funct, Genet. 2004; 54(2):247–259. [PubMed: 14696187] (c) Madan Babu M, Kumar Singh S, Balaram P. A C–H···O Hydrogen Bond Stabilized Polypeptide Chain Reversal Motif at the C Terminus of Helices in Proteins. J Mol Biol. 2002; 322(4):871–880. [PubMed: 12270720] (d) Derewenda ZS, Lee L, Derewenda U. The Occurence of C–H···O Hydrogen Bonds in Proteins. J Mol Biol. 1995; 252(2):248–262. [PubMed: 7674305] (e) Bonchev D, Cremaschi P. C-H Group as Proton Donor by Formation of a Weak Hydrogen Bond. Theoret Chim Acta. 1974; 35(1):69–80.

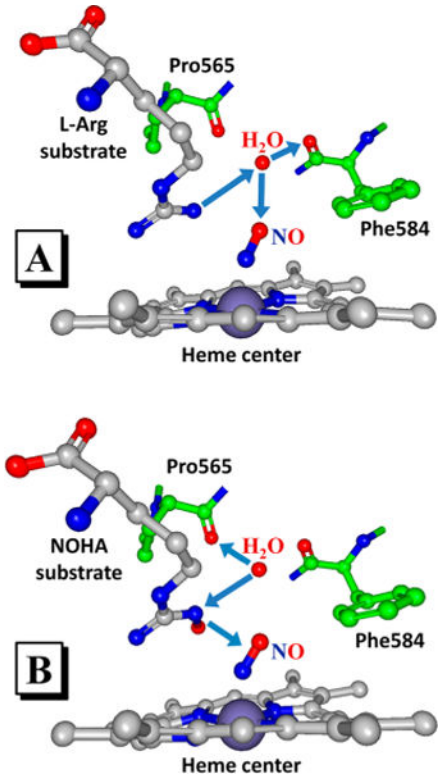


**Figure 1.**

Structures of heme active sites of nNOS/Arg (panel A, pdb 2G6K) and nNOS/NOHA (panel B, pdb 3HSP). The arrows show the potential H-bonds between the active site water, substrate, the NO ligand and nearby residues, as identified on the basis of the distance and angle considerations in the X-ray investigations[4] (the arrow direction is from the H-bond donor to the acceptor).

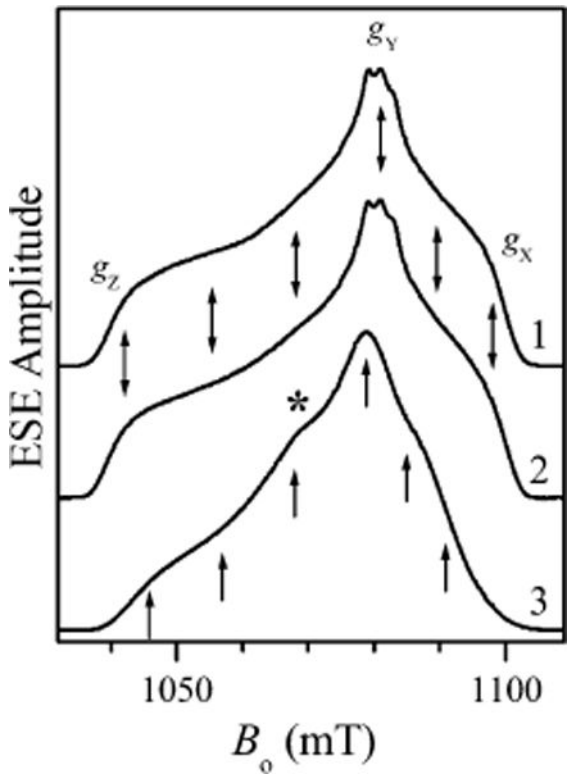


**Figure 2.**

Two-pulse ESE field sweeps of ferrous–NO heme centers in nNOS/NS (trace 1), nNOS/Arg (trace 2), and nNOS/NOHA (trace 3). The arrows indicate the EPR positions, at which the ENDOR spectra were measured. The $B_0$ values (in mT) corresponding to the indicated EPR positions: (1042, 1055, 1068, 1081, 1089.5, 1098) for nNOS/NS and nNOS/Arg and (1045.8, 1056.8, 1067.8, 1078.8, 1084.8, 1090.8) for nNOS/NOHA. Experimental conditions: mw frequency, 30.305 GHz; mw pulses, 15 and 22 ns; time interval between the mw pulses, $\tau = 200$ ns; temperature, 15 K. The asterisk indicates a commonly observed minor feature of unknown origin (see Figures S2 and S3 in the Supporting Information for a numerical simulation).

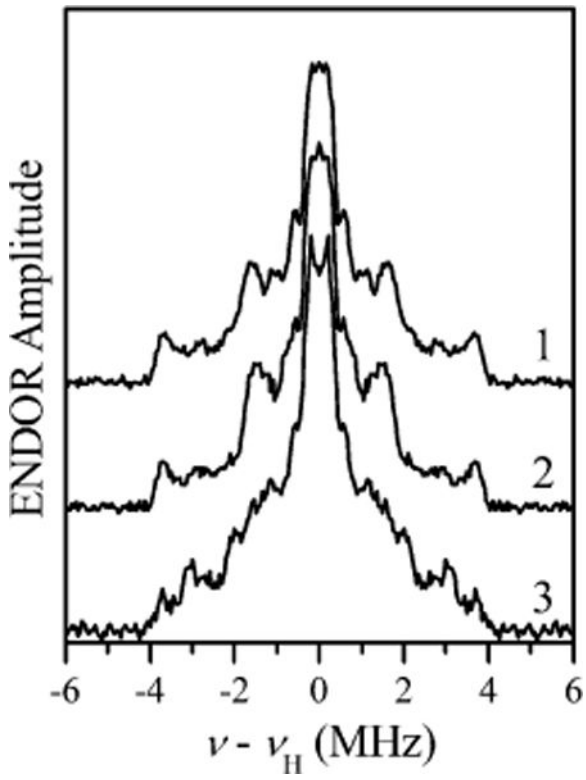


**Figure 3.**

Refocused Mims ENDOR spectra of nonexchangeable protons in the vicinity of ferrous–NO heme centers of nNOS/NS, nNOS/Arg, and nNOS/NOHA in $D_2O$ (traces 1–3, respectively) at the EPR position where the largest ENDOR splitting is observed ($B_0$ = 1068 mT for nNOS/NS and nNOS/Arg; $B_0$ = 1067.8 mT for nNOS/NOHA). Experimental conditions: mw frequency, 30.305 GHz; mw pulses, 15, 15, 15, and 22 ns; time interval between the first and second pulses, $\tau$ = 80 ns; time interval between the second and third pulses, T = 20 $\mu$s; time interval between the third and fourth pulses, $t$ = 280 ns; RF pulse length, 18 $\mu$s; temperature, 15 K.

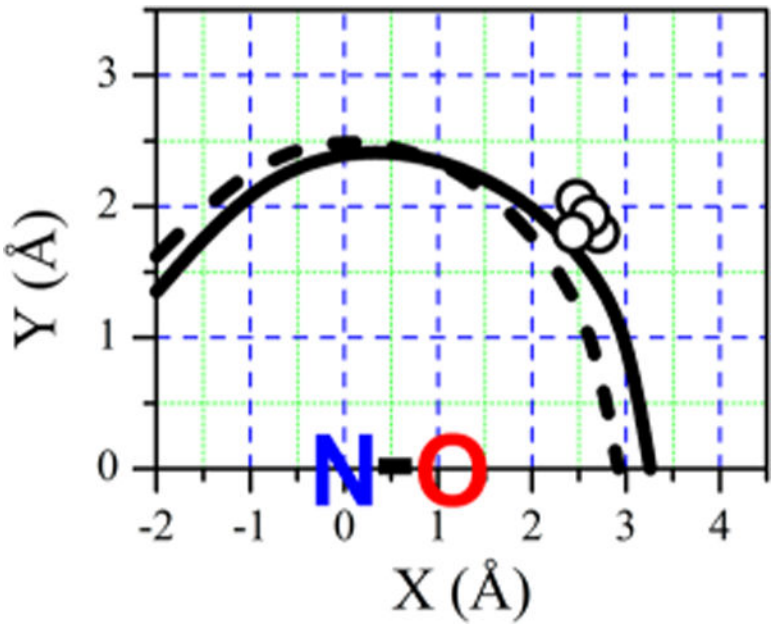


**Figure 4.**

Position of $H_{\varepsilon}$ of Phe584 with respect to the NO ligand. Black lines show the range of possible positions predicted on the basis of $T_{\|}$ = 7.65 MHz using the spin density distributions ($\rho_{Fe}$, $\rho_{N}$, $\rho_{O}$) = (0.2, 0.5, 0.3) (solid line) and ($\rho_{Fe}$, $\rho_{N}$, $\rho_{O}$) = (0.2, 0.7, 0.1) (dashed line). Open circles are the positions of Phe584 $H_{\varepsilon}$ in nNOS/Arg and nNOS/NOHA predicted from crystal structures (pdb 2G6K and 3HSP, respectively).

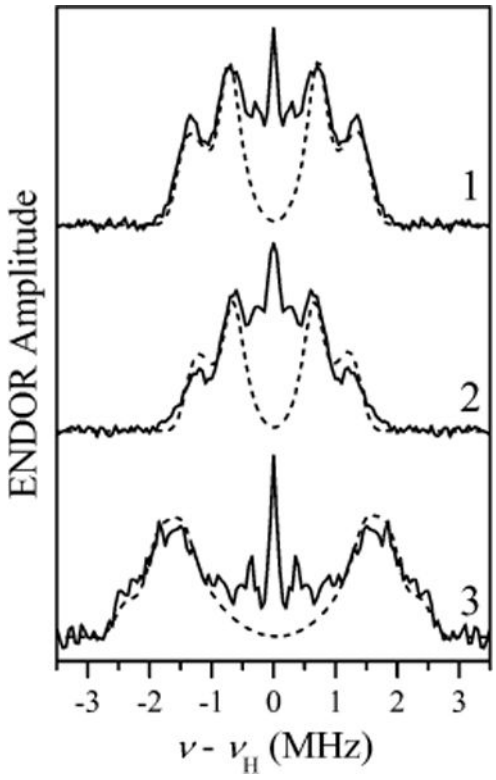


**Figure 5.**

Field-integrated refocused Mims ENDOR of exchangeable protons in the vicinity of ferrous–NO heme centers of nNOS/NS, nNOS/Arg, and nNOS/NOHA (traces 1–3, respectively). Solid traces are experimental results, obtained as differences between the ENDOR spectra of samples in $H_2O$ and $D_2O$ (the original orientation-selective spectra used to calculate the FI spectra are shown in Figure S4 of Supporting Information). Experimental conditions are the same as in Figure 3. Dashed traces are simulations with ($a_{iso}$, $T_{11}$, $T_{22}$, $T_{33}$) = (0, −1.55, −1.55, +3.1) MHz for nNOS/NS, (0, −1.4, −1.4, +2.8) MHz for nNOS/Arg, and (−0.6, −3.4, −2.3, +5.7) MHz for nNOS/NOHA. In the above notation, $T_{33}$ corresponds to $T_{||}$ used for simplicity in the text. The accuracy of $T_{33}$ is ±0.1 MHz, and the corresponding accuracy for $T_{11}$ and $T_{22}$ is ±0.05 MHz. The formal accuracy for $a_{iso}$ is ±0.05 MHz, but because the exchangeable protons for nNOS/NS and nNOS/Arg are beyond the H-bonding range (Figure 6), $a_{iso}$ in these samples is strictly zero for all practical purposes. Individual Gaussian line widths were 0.25 MHz in all simulations.

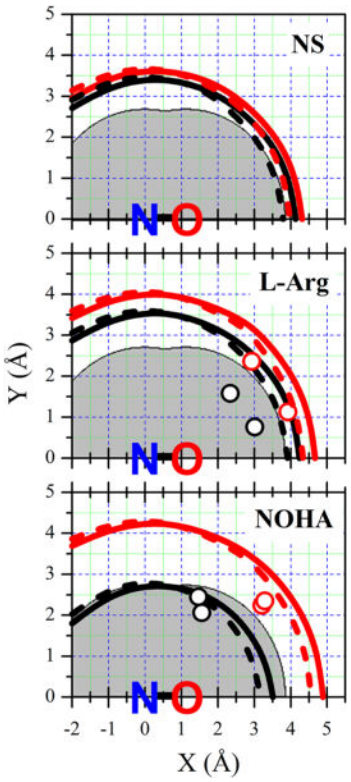


**Figure 6.**

Positions of the nearby exchangeable proton (black) and active site water oxygen (red) with respect to the NO ligand. Solid and dashed lines (calculated using ($\rho_{Fe}$, $\rho_{N}$, $\rho_{O}$) = (0.2, 0.5, 0.3) and (0.2, 0.7, 0.1), respectively) show the possible positions predicted on the basis of the experimental $T_{||}$ values. Open circles show the proton and oxygen positions predicted or directly read from crystal structures (pdb 2G6K and 3HSP).

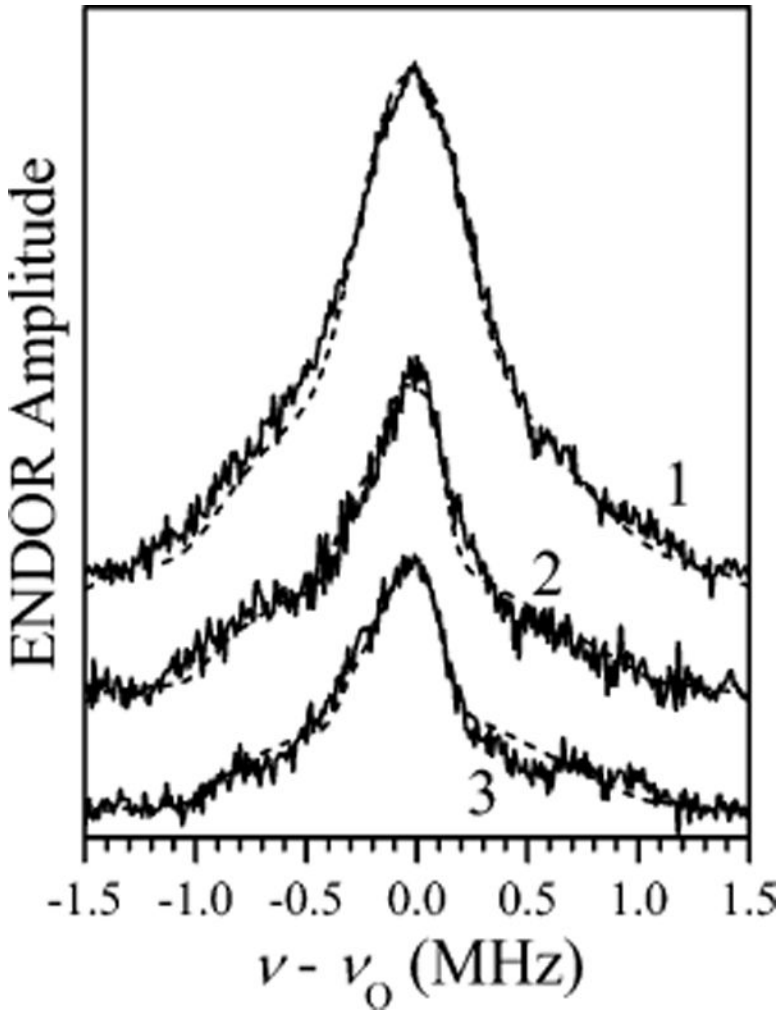


**Figure 7.**

Field-integrated Mims ENDOR spectra of exchangeable $^{17}O$ in the vicinity of ferrous–NO heme centers of nNOS/NS, nNOS/Arg, and nNOS/NOHA in $H_2{}^{17}O$ (traces 1–3, respectively). Solid traces are experimental results (the original orientation-selective spectra used to calculate the FI spectra are shown in Figure S5 of Supporting Information). Experimental conditions: mw frequency, 30.305 GHz; mw pulses, 15, 15, and 15 ns; time interval between the first and second pulses, $\tau$ = 700 ns; time interval between the second and third pulses, $T$ = 15 $\mu$s; RF pulse length, 10 $\mu$s; temperature, 15 K. Dashed traces are simulations with $a_{iso}$ = 0 (for all traces) and $T_{||}$ = −0.36 MHz for nNOS/NS, −0.27 MHz for nNOS/Arg, and −0.23 MHz for nNOS/NOHA. The *nqi* parameters were $e^2Qq/h$ = 6.5 MHz and $\eta$ = 1. The orientation of the *nqi* frame with respect to the *hfi* one is described by the Euler angles ($\theta_{hq}$, $\psi_{hq}$) = (60°, 30°), (40°, 50°), and (40°, 50°) for nNOS/NS, nNOS/Arg, and nNOS/NOHA, respectively (the angle $\phi_{hq}$ is arbitrary because the *hfi* tensor is axial. See the Supporting Information for the Euler angles definition). Individual Gaussian line widths were 0.2 MHz for nNOS/NS and 0.1 MHz for nNOS/Arg and nNOS/NOHA. See the

Supporting Information for the simulation details. Simulation examples using other parameters are also presented in Figures S6 and S7 of the Supporting Information.

**Table 1**

Distances to $N_{NO}$ and $O_{NO}$, and Estimated Anisotropic *hfi* Constants for the Nearest Non-Exchangeable Proton ($H_{\varepsilon}$ of F584) and the Oxygen Atom of the Active Site Water Molecule in the nNOS Subunits A and B[a]

| atom | dist to $N_{NO}$ (Å) | dist to $O_{NO}$ (Å) | $T_{\parallel}$ (MHz) for $\rho$ (Fe,N,O) = (0.2, 0.5, 0.3) | $T_{\parallel}$ (MHz) for $\rho$(Fe,N,O) = (0.2, 0.7, 0.1) | exptl $T_{\parallel}$ (MHz) |
|---|---|---|---|---|---|
| $^{1}H_{\varepsilon}$ of F584 in nNOS/NS | | | | | 7.65 |
| $^{1}H_{\varepsilon}$ of F584 in nNOS/Arg | 3.24 (3.03) | 2.41 (2.22) | 5.77 (7.19) | 4.55 (5.54) | 7.65 |
| $^{1}H_{\varepsilon}$ of F584 in nNOS/NOHA | 3.21 (3.25) | 2.43 (2.36) | 5.90 (5.94) | 4.67 (4.58) | 7.65 |
| $^{17}O_{H_2O}$ in nNOS/NS | | | | | −0.36 |
| $^{17}O_{H_2O}$ in nNOS/Arg | 3.76 (4.08) | 2.95 (2.99) | −0.46 (−0.42) | −0.38 (−0.32) | −0.27 |
| $^{17}O_{H_2O}$ in nNOS/NOHA | 3.92 (4.04) | 3.04 (3.16) | −0.42 (−0.38) | −0.35 (−0.31) | −0.23 |
| $^{15}N_{g1}$ in nNOS/Arg | 2.97 (3.07) | 3.06 (2.87) | −0.48 (−0.48) | −0.50 (−0.48) | −0.93 |
| $^{1}H_{exch}$ in nNOS/NS | | | | | 3.1 |
| $^{1}H_{exch}$ in nNOS/Arg | 2.8 (3.08) | 1.95 (1.99) | 9.88 (8.90) | 7.28 (6.00) | 2.8 |
| $^{1}H_{exch}$ in nNOS/NOHA | 2.58 (2.86) | 2.10 (2.47) | 8.96 (6.39) | 7.99 (5.89) | 5.7 |
| $^{1}H_{\delta}$ of L-Arg in nNOS/Arg | 3.06 (2.98) | 2.41 (2.57) | 6.11 (5.71) | 5.13 (5.23) | 2.35 |

[a]The structural parameters are obtained from pdb 2G6K and 3HSP. The distances and calculated $T_{||}$ values without and within parentheses correspond to subunits A and B, respectively. The experimental $T_{||}$ values for the L-Arg $^{1}H_{\delta}$ and $^{15}N_{g1}$ are from ref 16.